

# Controlling the Oxidation State of Cu Electrode and Reaction Intermediates for Electrochemical CO<sub>2</sub> Reduction to Ethylene

Tsu-Chin Chou<sup>1</sup>, Chiao-Chun Chang<sup>1</sup>, Hung-Ling Yu<sup>1</sup>, Wen-Yueh Yu<sup>2</sup>, Chung-Li  
Dong<sup>3</sup>, Juan-Jesús Velasco-Vélez<sup>4</sup>, Cheng-Hao Chuang<sup>3</sup>, Li-Chyong Chen<sup>1,5</sup>, Jyh-Fu  
Lee<sup>6</sup>, Jin-Ming Chen<sup>6</sup> and Heng-Liang Wu<sup>1,5\*</sup>

1. Center for Condensed Matter Sciences, National Taiwan University, Taipei 10617, Taiwan
2. Department of Chemical Engineering, National Taiwan University, Taipei 10617, Taiwan
3. Department of Physics, Tamkang University, New Taipei City 25137, Taiwan.
4. Department of Inorganic Chemistry, Fritz-Haber-Institut der Max-Planck-Gesellschaft, Berlin 14195, Germany
5. Center of Atomic Initiative for New Materials, National Taiwan University, Taipei 10617, Taiwan
6. National Synchrotron Radiation Research Center, Hsinchu, 30076, Taiwan

\*Corresponding author E-mail: [hengliangwu@ntu.edu.tw](mailto:hengliangwu@ntu.edu.tw)

KEYWORDS: Electrochemical CO<sub>2</sub> reduction, *in situ* SEIRAS, *in situ* soft X-ray  
absorption spectroscopy, CO intermediates, Oxidation state of Cu surface.

## Abstract:

Understanding the role of oxidation state of Cu surface and surface-adsorbed intermediate species in electrochemical CO<sub>2</sub> reduction is crucial for the development of selective CO<sub>2</sub>-to-fuel electrocatalysts. In this study, the electrochemical CO<sub>2</sub> reduction mechanism over the Cu catalysts with various oxidation states was studied by using *in situ* surface-enhanced infrared absorption spectroscopy (SEIRAS), *in situ* soft X-ray absorption spectroscopy (Cu L-edge) and on-line gas chromatography measurements. The atop-adsorbed CO (CO<sub>atop</sub>) intermediate is obtained on the electrodeposited Cu surface which primarily has the oxidation state of Cu(I). CO<sub>atop</sub> is further reduced, followed by the formation of C<sub>1</sub> product such as CH<sub>4</sub>. The residual bridge-adsorbed CO (CO<sub>bridge</sub>) is formed on the as-prepared Cu surface with Cu(0) which inhibits hydrocarbon formation. In contrast, the CV-treated Cu electrode prepared by oxidizing the as-prepared Cu surface contains different amount of Cu(I) and Cu(0) states. The major theme of this work is that *in situ* SEIRAS results show the coexistence of CO<sub>atop</sub> and CO<sub>bridge</sub> as the reaction intermediates during CO<sub>2</sub> reduction and the selectivity of CO<sub>2</sub>-to-ethylene conversion is further enhanced in the CV-treated Cu electrode. The Cu catalysts modulated by electrochemical method exhibit different oxidation states and reaction intermediates as well as the electrocatalytic properties.

## Introduction

Electrochemical CO<sub>2</sub> reduction reaction (CO<sub>2</sub>RR) is a promising route to convert CO<sub>2</sub> into valuable hydrocarbon fuels and chemical feedstock for sustainable carbon cycles.<sup>1-2</sup> The catalysts capable of electrochemically reducing CO<sub>2</sub> still suffer from many challenges such as short catalyst lifetime, high overpotential, low Faradic efficiencies (FEs) and poor product selectivity, mainly due to the multiple number of proton-coupled electron transfer steps.<sup>3</sup> The development of efficient and selective catalysts for CO<sub>2</sub>RR has attracted tremendous attentions.<sup>4-6</sup> Among all transition metal catalysts explored for CO<sub>2</sub>RR, copper (Cu) is the promising catalyst to produce hydrocarbons including methane (CH<sub>4</sub>) and ethylene (C<sub>2</sub>H<sub>4</sub>).<sup>7-8</sup> However, bulk Cu electrode exhibits high overpotentials and a lack of product selectivity. Furthermore, metallic Cu is oxidized under air easily.

Various strategies have been used to enhance the performance of CO<sub>2</sub>RR performance by modulating the catalytic structure and physical properties of electrolyte as well as the oxidation state of Cu catalyst.<sup>4, 6, 9-14</sup> For instance, Cu nanostructures with different particle size, particle morphology and surface area exert a great impact on the catalytic properties.<sup>9-14</sup> C<sub>2</sub> products are formed over the Cu(100) electrode while Cu(111) is effective to produce C<sub>1</sub> products,<sup>7-8</sup> suggesting that the facet of Cu catalyst results in different CO<sub>2</sub> reduction mechanisms. The physical properties of electrolyte

also play crucial roles in the product selectivity over the Cu electrodes. The electrolyte with different proton concentrations (pH values) influences the protonation step for the production of COOH in CO<sub>2</sub>RR.<sup>5</sup>

The product selectivity can be enhanced over the oxide-derived Cu catalysts.<sup>11, 13, 15-18</sup> These Cu-based materials synthesized by the reduction of thermally oxidized Cu,<sup>19</sup> electrodeposited Cu<sub>2</sub>O,<sup>20</sup> and oxygen plasma treated Cu catalysts<sup>13, 18</sup> display a higher current density, formation of CO at low overpotentials, and improved FEs of C<sub>2</sub>H<sub>4</sub>.<sup>18</sup> The effect of the oxide-derived Cu catalysts on the product selectivity has been studied. The grain boundaries in oxide-derived Cu could provide unique surface sites.<sup>21-22</sup> Reske *et al.* showed that the low-coordinated atoms formed on the surface of the catalyst behave as the active sites during the oxide reduction.<sup>9</sup> The Cu<sup>δ+</sup> sites remained on the oxide-derived Cu surface have also been suggested to be the active sites for CO<sub>2</sub>RR.<sup>18, 20</sup> To further examine the effect of Cu(I) on the CO<sub>2</sub> reduction mechanism, previous studies reported that Cu(I) sites alone do not improve the efficiencies of CO<sub>2</sub>RR. The DFT calculations proposed that the synergy between active surface Cu(I) and Cu(0) regions resulted in the adsorption of CO intermediates on different reaction sites is responsible for improving the CO dimerization.<sup>23</sup> However, experimental evidences are needed for the proposed model.

The surface-adsorbed CO intermediates are formed during CO<sub>2</sub>RR, followed by

the dimerization process of CO intermediates, which are generally regarded as the control step for CH<sub>4</sub> and C<sub>2</sub>H<sub>4</sub> formation.<sup>5</sup> *In situ* surface-enhanced infrared absorption spectroscopy (SEIRAS) is a powerful tool for examining the adsorbed intermediates on Cu catalysts.<sup>24-28</sup> As a result of various adsorption sites for CO molecule, previous studies on Cu surface mainly focus on the dynamic evolution of adsorbed CO and the formation of adsorbed CO including atop-adsorbed CO and bridge-adsorbed CO.<sup>27, 29-30</sup> The atop-adsorbed CO has been recognized as the common intermediate on Cu surface<sup>24-28</sup> and the atop-adsorbed CO alone is observed in a variety of experimental conditions such as pH value of electrolyte,<sup>31</sup> and partial pressure of CO<sub>2</sub> (or CO).<sup>25</sup> These Cu electrodes are electrochemically deposited on Au substrate and chemically deposited on Si prism.<sup>26, 32</sup> In contrast, Gunathunge *et al.* showed that both atop-adsorbed CO and bridge-adsorbed CO can be formed on the chemically deposited Cu thin film in alkaline pH electrolyte and the bridge-adsorbed CO is inactive during CO<sub>2</sub>RR.<sup>27</sup> In addition, these CO intermediates are also observed in electropolished Cu electrode,<sup>30</sup> suggesting that controlling the formation of atop-adsorbed CO and bridge-adsorbed CO on Cu surface is still challenging. The CO<sub>2</sub> reduction mechanism behind various Cu electrodes is unclear due to the lack of understanding of oxidation state of Cu accompanied with the formation of CO intermediates.

In this study, we used *in situ* soft X-ray absorption spectroscopy, *in situ* SEIRAS

and on-line gas chromatography (GC) measurements to study the oxidation state of Cu, surface-adsorbed intermediates and final products during CO<sub>2</sub>RR. By combining these *in situ* techniques, we are able to provide the complementary information and elucidate the reaction pathways about the electrochemical CO<sub>2</sub> reduction mechanism on Cu electrodes. Our results show that the amount of Cu(I) and Cu(0) oxidation states in Cu catalysts can be modulated by the electrochemical method. The coexistence of atop-adsorbed CO and bridge-adsorbed CO on the CV-treated Cu surface is observed during CO<sub>2</sub> reduction. The different CO species formed on the Cu electrodes could play crucial roles in the CO<sub>2</sub> reduction mechanism. The prepared Cu electrodes with specific oxidation states influence the formation of CO intermediates and product selectivity during CO<sub>2</sub>RR.

## Experimental Section

### Chemicals and electrolyte

KHCO<sub>3</sub> (≥99.8 %) and CuSO<sub>4</sub> (≥99.8 %) were purchased from Sigma Aldrich. Ultrapure H<sub>2</sub>SO<sub>4</sub> (98 %) and CO<sub>2</sub> (≥99.995 %) were purchased from Kanto Chemical Co. and FMI gas Taiwan, respectively. All chemicals were used as received without further purification. Millipore triple-distilled water (18.2 MΩ) was used to prepare solutions. The 0.1 M CO<sub>2</sub>-saturated KHCO<sub>3</sub> electrolyte with a pH value of 6.8 is prepared by purging CO<sub>2</sub> in 0.1 M KHCO<sub>3</sub> electrolyte for 60 min.

### **Preparation of as-prepared Cu electrodes**

A Cu thin film with the thickness of ca. 36 nm was prepared using physical vapor deposition (PVD) on the reflecting plane of hemicylindrical Si prism or Si wafer by a home-built ion beam sputtering system and then transferred into the electrochemical cell immediately for the measurements to avoid the Cu oxidation. The thickness of as-prepared polycrystalline Cu was measured by atomic force microscopy (AFM, Figure S1). A high purity Cu (99.998 %) purchased from Gredmann Taiwan Ltd. is used as the sputtering target and Ar<sup>+</sup> is serving as the bombardment source. The deposition rate and thickness are monitored by using a quartz crystal microbalance. The as-prepared Cu electrode was deposited at a deposition rate of 0.4 Å s<sup>-1</sup> in the present study.

### **Preparation of cyclic voltammetry (CV)-treated Cu electrodes**

CV-treated Cu electrode is prepared by cycling the as-prepared Cu electrode in a potential region of 0.55 to -0.3 V. All potentials in the present study are reported with respect to the reversible hydrogen electrode (RHE).

### **Preparation of electrodeposited Cu on Au electrode**

A thin Au film with a thickness of ~ 10 nm is prepared on Si prism using electroless deposition described previously.<sup>24, 26, 33</sup> The Au film was cycled in an Ar-saturated 0.1 M H<sub>2</sub>SO<sub>4</sub> solution at a scan rate of 50 mV s<sup>-1</sup> between 0.1 and 1.6 V (vs. RHE) to clean Au surface.<sup>34</sup> The prepared Au film was then transferred in a solution of 5 mM CuSO<sub>4</sub>

and 0.1 M H<sub>2</sub>SO<sub>4</sub> for the electrochemical deposition process. Cu film (~50 nm) was then electrochemically deposited on Au film at 0.1 V (vs. RHE) for 600 s.<sup>26</sup> Figure S2 shows the AFM image and CV of electrodeposited Cu.

### ***In situ* surface-enhanced infrared absorption spectroscopy and electrochemical measurements**

*In situ* surface-enhanced infrared absorption spectroscopy (SEIRAS) was recorded in the home-built reflection accessory with external reflection configuration using a Thermo Nicolet 6700 FTIR spectrometer equipped with a HgCdTe (MCT) detector.<sup>35</sup> All spectra were acquired with a spectral resolution of 4 cm<sup>-1</sup>. The typical acquisition time was 30 s per spectrum. The time-dependent measurement takes 12 s per spectrum. For spectroelectrochemical measurements, the spectrometer was coupled with the electrochemical workstation (ZENNIUM E, Zahner). The working electrodes are PVD Cu or electrodeposited Cu on Au. The counter and reference electrodes are graphite rod and Ag/AgCl electrode, respectively. The graphite counter electrode is used to avoid any possible contaminations from Pt electrode.<sup>26</sup> The electrolytes used in all spectroelectrochemical measurements were 0.1 M CO<sub>2</sub>-saturated KHCO<sub>3</sub> (pH = 6.8). The CV for *in situ* SEIRAS measurements was performed at a scan rate of 2 mV s<sup>-1</sup>. Figure S3 shows the cell configuration of *in situ* SEIRAS measurements. More details for *in situ* SEIRAS are described elsewhere.<sup>36</sup>



## X-ray absorption spectroscopy measurements

*In situ* soft X-ray absorption spectroscopy was used to monitor the changes in oxidation state of Cu surface during reactions. *In situ* and *ex situ* Cu L<sub>3</sub>-edge X-ray absorption spectroscopy measurements were conducted with total fluorescence yield (TFY) mode and total electron yield (TEY) mode, respectively, in Taiwan Light Source beam-line 20A end station (National Synchrotron Radiation Research Center, Taiwan). A flow type spectroelectrochemical cell was used for *in situ* soft X-ray absorption spectroscopy measurements as described in previous literature.<sup>37</sup> First, we deposit Cu thin film (PVD Cu) with the thickness of ~36 nm on a SiN<sub>x</sub> X-ray transparent window with underlying adhesion layers of Cr (2 nm) and Au (5 nm) served as working electrodes, and two Pt wires were conducted as counter and reference electrodes. X-ray absorption spectra were collected as a function of applied potential during cyclic voltammetry (CV) at a scan rate of 2 mV s<sup>-1</sup>, which yields a potential resolution of ~120 mV owing to an acquisition time of 60 s per spectrum. Figure S4 shows the cell configuration of *in situ* soft X-ray absorption spectroscopy measurements. Since the Cu electrodes can be easily oxidized under air conditions, all the prepared Cu electrodes were kept in a vacuum chamber and transferred to a chamber filled with Argon before the soft X-ray absorption spectroscopy measurements to avoid the Cu oxidation.

*In situ* Cu K-edge X-ray absorption spectroscopy including extended X-ray

absorption fine-structure spectroscopy (EXAFS) was conducted in Taiwan Light Source beam-line 17A end station (National Synchrotron Radiation Research Center, Taiwan). All the spectra were further analyzed with Athena software.

### **Atomic force microscopy**

The surface morphology of Cu was imaged by atomic force microscopy (AFM, Innova, Bruker) with tapping mode by using a Si<sub>3</sub>N<sub>4</sub> cantilever (TESPA, radius of 8 nm, spring constant of 42 N m<sup>-1</sup>, resonance frequency of 320 kHz, Bruker). All AFM studies were conducted on Si prisms with a hemicylindrical holder.

### **High performance liquid chromatography and on-line gas chromatography measurements**

Gas product analysis was carried out using home-built on-line gas chromatography (GC) system with pulsed discharge helium ionization detector. (Agilent 7890, USA) The electrochemical cell coupled to the GC system was used to monitor the gas products formed during CO<sub>2</sub> reduction. Figure S5 shows the cell configuration for on-line GC measurements. High performance liquid chromatography (HPLC) with photometric diode array detector (JASCO, Japan) was used to analyze the liquid products such as formic acid (HCOOH). The reaction potential was held for 5 min to accumulate enough product for each GC/HPLC measurement. Each measurement takes ~20 min. Both PVD Cu electrode and electropolished Cu foil were used to study the

effect of CV treatment on the product distributions. The electropolished Cu foil was held at -1 V for 60 min to form the as-prepared Cu foil with the oxidation state of Cu(0) in the CO<sub>2</sub>-saturated 0.1 M KHCO<sub>3</sub> electrolyte. The calculation of Faradaic efficiencies (FEs) for gas and liquid products is shown in supporting information.

## Results and Discussion:

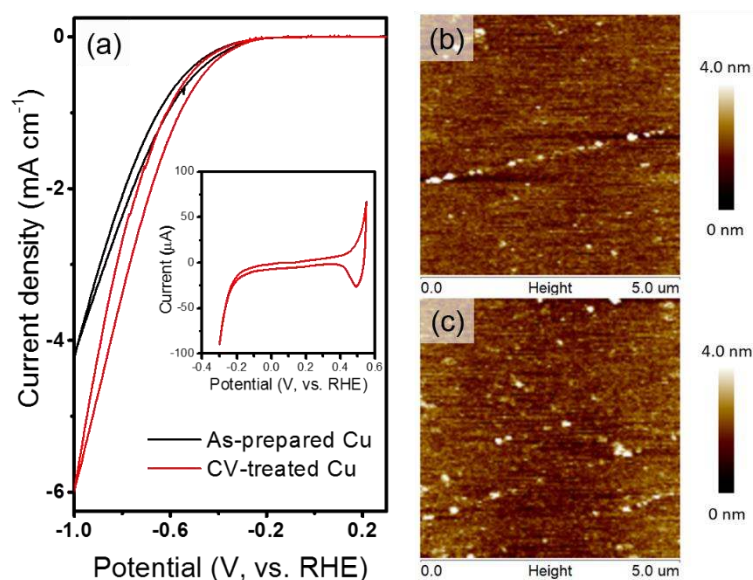


**Figure 1.** (a) Cyclic voltammetry (CV) of as-prepared Cu electrode and CV-treated Cu electrode with CO<sub>2</sub>-saturated 0.1 M KHCO<sub>3</sub> electrolyte at a scan rate of 10 mV s<sup>-1</sup> in the potential range of 0.25 and -1 V. The inset in Figure 1a: CV curve of as-prepared Cu electrode obtained in a potential range of -0.3 to 0.55 V. AFM images of the surface morphology of (b) as-prepared and (c) CV-treated Cu electrode (after three CV-treated cycles). The scanned area of AFM images is 5 μm x 5 μm.

Figure 1a shows the cyclic voltammetry (CV) of as-prepared Cu electrode and CV-treated Cu electrode with CO<sub>2</sub>-saturated 0.1 M KHCO<sub>3</sub> electrolyte at a scan rate of 10 mV s<sup>-1</sup> in the potential range of 0.25 to -1 V. The as-prepared Cu electrode is cycled in the potential region of 0.55 to -0.3 V (inset in figure 1a). After three cycles, CV-treated

Cu electrode is prepared and exhibits a larger reduction current than that of as-prepared Cu electrode in CO<sub>2</sub>-saturated 0.1 M KHCO<sub>3</sub> electrolyte. Figure 1b-c shows the AFM images of the surface morphology of (b) as-prepared and (c) CV-treated Cu electrode (after three CV-treated cycles) with a scanned area of 5 μm x 5 μm. The surface roughness of CV-treated Cu electrode is similar to that of as-prepared Cu surface ( $R_q = 0.44 \pm 0.05$  nm for as-prepared Cu surface and  $R_q = 0.50 \pm 0.04$  nm for CV-treated Cu surface), suggesting that the changes in surface area of Cu electrode have less contribution on the larger reduction current of CV treated Cu surface during CO<sub>2</sub> reduction. Meanwhile, the double layer capacitances obtained from Cu electrodes suggest less changes in surface area of as-prepared Cu after three CV-treated cycles (Figure S6).

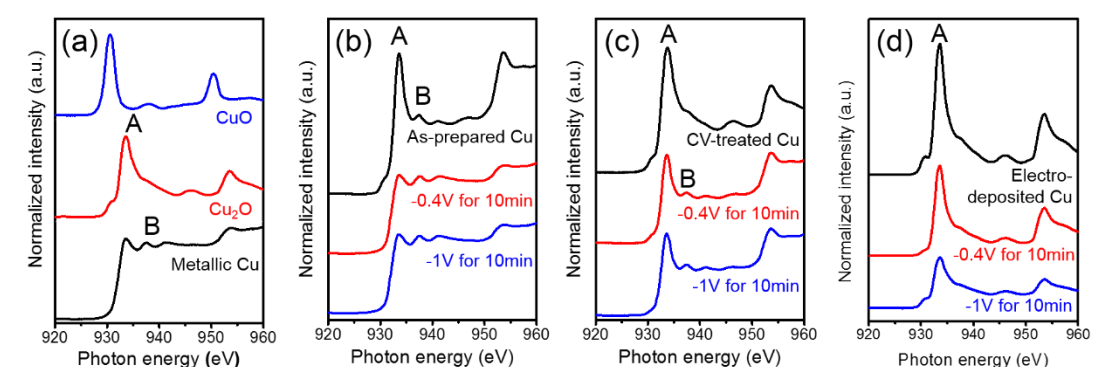


**Figure 2.** (a) Cu L<sub>3</sub>-edge X-ray absorption spectra (XAS)-TEY mode of standard Cu electrodes. *Ex situ* Cu L<sub>3</sub>-edge XAS of (b) as-prepared Cu electrode, (c) CV-treated Cu electrode (after three CV-treated cycles), and (d) electrodeposited Cu electrode obtained before and after CO<sub>2</sub> reduction. The XAS were collected in TEY mode.

To study the oxidation state of different Cu surfaces, *ex situ* Cu L<sub>3</sub>-edge soft X-ray absorption spectroscopy were used to reveal the changes in oxidation state of Cu

electrode prepared at representative potentials with CO<sub>2</sub>-saturated 0.1 M KHCO<sub>3</sub> electrolyte. As compared to Cu K-edge hard X-ray absorption spectroscopy, the soft X-ray absorption spectroscopy measurements collected in TEY mode can be used to study the oxidation state of Cu surface in a range of 2-20 nm thickness which provides surface information.<sup>38-39</sup> Figure 2a shows Cu L<sub>3</sub>-edge X-ray absorption spectra (XAS)-TEY mode of Cu, Cu<sub>2</sub>O and CuO electrodes as the reference spectra.<sup>37, 40</sup> Peak A at 933.6 eV is associated with the feature of Cu(I) and peak B at 937.5 eV is assigned to the metallic Cu (Cu(0)) in Cu electrode.<sup>37, 40</sup> Figure 2b-d shows Cu L<sub>3</sub>-edge XAS of (b) as-prepared Cu electrode, (c) CV-treated Cu electrode (after three CV-treated cycles), and (d) electrodeposited Cu electrode in TEY mode. The feature of peak A and B suggests that both Cu(0) and Cu(I) exist on the surface of as-prepared Cu electrode before CO<sub>2</sub> reduction. (Fig. 2b) Thus, the XAS of as-prepared Cu electrode also exhibit Cu(I) feature before CO<sub>2</sub>RR. The existence of Cu(I) resulted from the surface oxidation of metallic copper under air conditions prior to immersion in the electrolyte has been proposed previously.<sup>41-42</sup> The XAS of the electrodeposited Cu electrode and CV-treated Cu electrode indicate that Cu(I) dominates the Cu surface before CO<sub>2</sub>RR and the Cu(0) feature could be embedded in the spectra. (Fig. 2c-d)

The prepared Cu electrodes are then held at representative potentials for 10 min during CO<sub>2</sub> reduction. Figure 2b-d show that *ex situ* Cu L<sub>3</sub>-edge XAS of (b) as-prepared

Cu electrode, (c) CV-treated Cu electrode, and (d) electrodeposited Cu electrode collected in TEY mode were obtained at representative potentials with CO<sub>2</sub>-saturated 0.1 M KHCO<sub>3</sub> electrolyte. The oxidation state of as-prepared Cu electrode changes from the mixture of Cu(0) and Cu(I) to Cu(0) at -0.4 V while the XAS of other two Cu catalysts are mainly showing the feature of Cu(I). The diminished Cu(I) at lower overpotential could be related to the small amount of Cu(I) in as-prepared Cu electrode. After further reduction at -1 V, the XAS of CV-treated Cu exhibit that the intensity of peak A decreases and the feature of peak B becomes clear after holding the potential at -1 V for 10 min, suggesting that some Cu(I) are reduced to Cu(0) and both Cu(I) and Cu(0) still exist on the Cu surface. In contrast, although the electrodeposited Cu should also contain the Cu(0) oxidation state during the reaction, XAS of electrodeposited Cu mainly exhibit the Cu(I) feature after holding the potential at -1 V for 10 min. The reduction from Cu(I) to Cu(0) in electrodeposited Cu electrode takes longer time than that of the other Cu electrodes which could be attributed to the larger amount of Cu(I) on electrodeposited Cu surface.

The hard X-ray absorption spectroscopy (Cu K-edge) was used to characterize the changes in oxidation state of Cu materials.<sup>18</sup> Figure S7 shows the Cu K-edge XAS of electrodeposited Cu electrode, as-prepared electrode and CV-treated Cu electrode. Although Cu K-edge XAS involve the information about the oxidation state of bulk Cu

metal ( $>2 \mu\text{m}$ ),<sup>43</sup> extended X-Ray absorption fine structure (EXAFS) obtained on the as-prepared Cu electrode shows the peak at  $2.2 \text{ \AA}$  which is assigned to the Cu-Cu bond.<sup>44-45</sup> EXAFS of electrodeposited Cu electrode and CV-treated Cu electrode shows the peak at  $1.5 \text{ \AA}$  associated with Cu-O bond, suggesting that Cu(I) could result from the persistence of Cu oxides.<sup>18</sup>

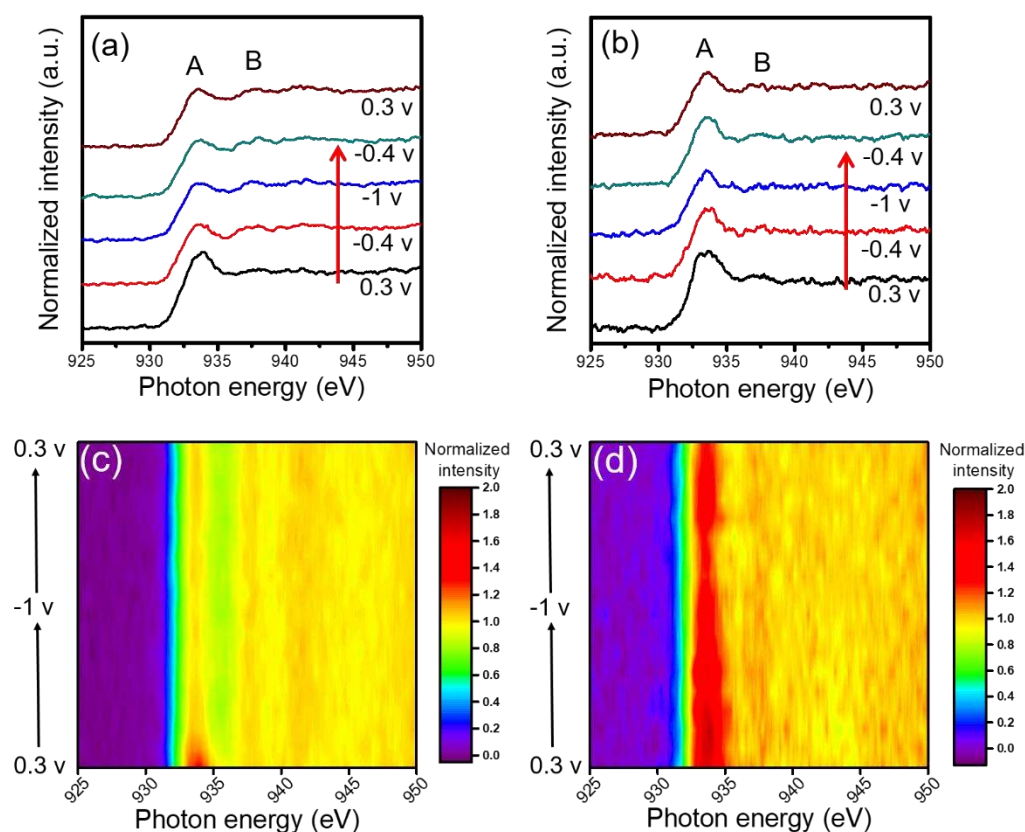


**Figure 3.** *In situ* Cu L<sub>3</sub>-edge XAS of (a) as-prepared Cu electrode, (b) CV-oxidized Cu electrode shown at representative potentials with CO<sub>2</sub>-saturated 0.1 M KHCO<sub>3</sub>. Contour plots of *in situ* Cu L<sub>3</sub>-edge XAS of (c) as-prepared Cu and (d) CV-treated Cu cycled between 0.3 and -1 V. *In situ* Cu L<sub>3</sub>-edge XAS were collected in TFY mode.

To further examine the effect of CV treatment on the characteristics of Cu electrode during electrochemical CO<sub>2</sub> reduction, we next performed *in situ* soft X-ray

absorption spectroscopy measurements of as-prepared Cu electrode and CV-treated Cu electrode to reveal the changes in oxidation state of Cu surface during electrochemical CO<sub>2</sub> reduction. Although the information provided by XAS-TEY mode is more surface sensitive, electrochemical soft X-ray absorption measurements can be operated in TFY mode.<sup>46</sup> We show the XAS-TFY mode of standard Cu electrodes in Figure S8. *In situ* Cu L<sub>3</sub>-edge XAS of as-prepared Cu electrode shown at representative potentials were obtained in the potential region of 0.3 and -1 V (Figure 3a). The scan rate is 2 mV s<sup>-1</sup> during cycling and the electrolyte is CO<sub>2</sub>-saturated 0.1 M KHCO<sub>3</sub>. Peak A at 933.6 eV associated with the feature of Cu(I) appears at 0.3 V.<sup>41</sup> During the CO<sub>2</sub> reduction process, the intensity of Peak A decreases during the scan from 0.3 to -1 V, indicating that the oxidation state of Cu surface changes from Cu(I) to metallic Cu. The oxidation state of as-prepared Cu electrode persists Cu(0) during the backward scan from -1 to 0.3 V. In contrast, *in situ* Cu L<sub>3</sub>-edge XAS of CV-treated Cu (after three CV-treated cycles) still exhibit the combination of Cu(I) and Cu(0) feature during cycling (Figure 3b).

Figure 3c-d shows the contour plots of *in situ* Cu L<sub>3</sub>-edge XAS of (c) as-prepared Cu and (d) CV-treated Cu cycled between 0.3 and -1 V with CO<sub>2</sub>-saturated 0.1 M KHCO<sub>3</sub> electrolyte. *In situ* Cu L<sub>3</sub>-edge XAS of as-prepared Cu show that the intensity of Cu(I) decreases rapidly during CO<sub>2</sub> reduction process (Figure 3c). In contrast, Figure 3d shows that the feature of Cu(I) obtained at 0.3 V becomes weaker during cycling.



We found that the reduction of Cu(I) to Cu(0) in CV-treated Cu is much slower, suggesting that the reduction of oxidation state over these Cu electrodes is a time-dependent process during CO<sub>2</sub> reduction.

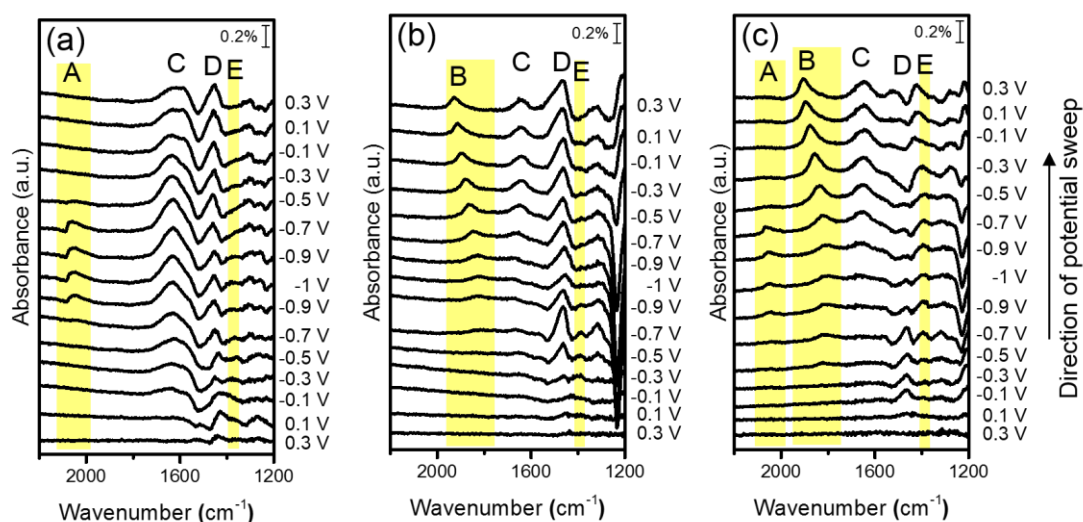


**Figure 4.** *In situ* SEIRAS of (a) electrodeposited Cu electrode, (b) as-prepared Cu electrode and (c) CV-treated Cu electrode (after three CV-treated cycles) during cathodic (negative) scan and anodic (positive) scan in CO<sub>2</sub>-saturated 0.1 M KHCO<sub>3</sub> electrolyte.

In order to understand the effect of valance state of Cu surface on the CO<sub>2</sub> reduction mechanism, we used *in situ* surface-enhanced infrared absorption spectroscopy (SEIRAS) to identify the intermediates formed on different Cu surface during CO<sub>2</sub> reduction. IR spectra were collected every 100 mV during a potential step. All the IR spectra are shown in Figure S9. Figure 4 shows *in situ* SEIRA spectra of (a) electrodeposited Cu electrode, (b) as-prepared Cu electrode and (c) CV-treated Cu electrode obtained at representative potentials during the first cycle. Reference spectra were obtained at 0.3 V in CO<sub>2</sub>-saturated 0.1 M KHCO<sub>3</sub> electrolyte. Figure 4a shows the

*in situ* SEIRA spectra of electrodeposited Cu electrode collected in the cathodic (negative) scan from 0.3 to -1 V. Peak A at 2048  $\text{cm}^{-1}$  corresponding to atop-adsorbed CO ( $\text{CO}_{\text{atop}}$ ) on Cu surface appears during the negative scan. The asymmetric peak A is observed as the potential is shifted to -1 V.<sup>47</sup>  $\text{CO}_{\text{atop}}$  disappears during the anodic (positive) scan. Among various adsorbed CO species,  $\text{CO}_{\text{atop}}$  is formed alone on the electrodeposited Cu surface during  $\text{CO}_2$  reduction.<sup>24, 26</sup> The position of  $\text{CO}_{\text{atop}}$ -associated peak obtained on Cu surface (2080-2040  $\text{cm}^{-1}$ ) is different from the position of  $\text{CO}_{\text{atop}}$ -associated peak obtained on Au surface (2110-2130  $\text{cm}^{-1}$ ),<sup>48</sup> suggesting that the electrodeposited Cu electrode completely covers the underlying Au surface.

In contrast, Figure 4b shows the *in situ* SEIRA spectra of as-prepared Cu electrode, clearly revealing peak B at 1832  $\text{cm}^{-1}$  during negative scan. Peak B associated with bridge-adsorbed CO ( $\text{CO}_{\text{bridge}}$ ) on Cu surface is obtained at -0.5 V and gradually redshifts to 1827  $\text{cm}^{-1}$  at -1 V during the negative scan. Upon scanning the potential from -1 to 0.3 V, peak B then blueshifts from 1827 to 1930  $\text{cm}^{-1}$ . Similar potential-dependent behavior of surface-adsorbed  $\text{CO}_{\text{bridge}}$  has been reported on Cu.<sup>27</sup> The blueshift in vibrational frequency of  $\text{CO}_{\text{bridge}}$  is ascribed to the decrease in the dipole-dipole interaction among  $\text{CO}_{\text{bridge}}$  molecules and/or electron back-donation from the Cu surface to the  $\text{CO}_{\text{bridge}}$  molecules.<sup>27, 49</sup> Peak C is associated with the H-O-H bending mode of adsorbed water on the Cu surface and peak D is assigned to  $\text{HCO}_2^-$ .<sup>35 50-51</sup> The

irreversible changes in the adsorption behavior of adsorbed water during cycling is consistent with previous studies.<sup>35</sup> The role of adsorbed water in CO<sub>2</sub> reduction mechanism is discussed in supporting information.

Interestingly, *in situ* SEIRA spectra of CV-treated Cu electrode show the formation of both CO<sub>atop</sub> and CO<sub>bridge</sub> during CO<sub>2</sub> reduction, suggesting that CO<sub>2</sub> reduction mechanism over the as-prepared Cu surface is changed after the CV treatment (Figure 2c). Although porous Cu materials effectively enhance vibrational signatures of surface adsorbates, which allows us to probe surface species,<sup>52</sup> the AFM images of as-prepared Cu surface and CV-treated Cu surface (after three CV-treated cycles) show a similar roughness of the Cu surfaces and the IR intensities of CO<sub>bridge</sub>-associated peaks obtained over the two Cu electrodes are the same. Thus, the appearance of CO<sub>atop</sub> in CV-treated Cu surface resulted from different plasmonic absorption properties of Cu surface can be excluded. In addition, peak E associated with COO<sup>-</sup> is formed, followed by the formation of CO<sub>atop</sub> and CO<sub>bridge</sub>. The intensity of peak E decreases in further reduction. Peak assignments are summarized in Table 1.<sup>24-29, 50-51, 53-54</sup>

Figure S10 shows the *in situ* SEIRA spectrum of CV-treated Cu electrode obtained at -1 V, exhibiting that both CO<sub>bridge</sub> and CO<sub>atop</sub> adsorbed on the Cu surface. We then remove the potential control and replace the electrolyte with fresh CO<sub>2</sub>-saturated 0.1 M KHCO<sub>3</sub> electrolyte without exposing the Cu electrode to air. On the measured anew

SEIRA spectrum of CV-treated Cu electrode, the  $\text{CO}_{\text{atop}}$ -associated peak disappears.

The fact that  $\text{CO}_{\text{atop}}$  can be removed from the surface without the applied potential

suggests that the formation of  $\text{CO}_{\text{atop}}$  on the Cu surface is a dynamic adsorption process.

Peak label	Peak position ( $\text{cm}^{-1}$ )	Assignments	Literature reference
A	1951~2094	CO stretching in atop adsorbed CO	24-29
B	1806~1907	CO stretching in bridge adsorbed CO	27-29
C	1645	H-O-H bending of $\text{H}_2\text{O}$	25, 26
D	1467	C-O stretching of $\text{HCO}_2^-$	50, 51
E	1396	$\text{COO}^-$ symmetric stretching	24, 53, 54

**Table 1.** Experimental vibrational frequencies and assignments for the species in electrochemical  $\text{CO}_2$  reduction.

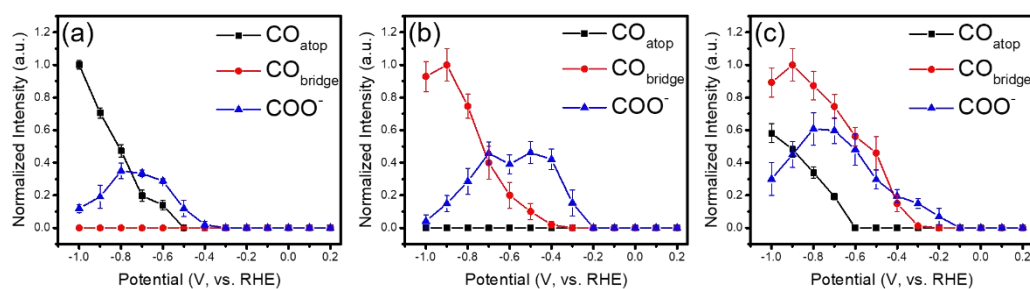


**Figure 5.** Potential dependence of the intensity of  $\text{CO}_{\text{atop}}$ ,  $\text{CO}_{\text{bridge}}$  and  $\text{COO}^-$  obtained in (a) electrodeposited Cu electrode, (b) as-prepared Cu electrode and (c) CV-treated Cu electrode from 0.2 to -1 V taken from Figure 4.

Figure 5 shows the potential dependence of the intensity of  $\text{CO}_{\text{bridge}}$ ,  $\text{CO}_{\text{atop}}$  and  $\text{COO}^-$  obtained in (a) electrodeposited Cu electrode, (b) as-prepared Cu electrode and (c) CV-treated Cu electrode from 0.2 to -1 V taken from Figure 4. All peak intensities were normalized to the most intense peak at specific potential. The  $\text{CO}_{\text{atop}}$ -associated peak is observed at -0.6 V and drastically increases from -0.6 to -1 V in electrodeposited Cu electrode (Figure 5a). The peak associated with  $\text{COO}^-$  appears at -0.4 V and gradually increases in further reduction. Figure 5b shows that  $\text{CO}_{\text{bridge}}$ -associated peak appears at -0.4 V in the as-prepared Cu electrode, while  $\text{CO}_{\text{atop}}$ -associated peak is absent

during the CO<sub>2</sub> reduction. Notably, both CO<sub>bridge</sub> and CO<sub>atop</sub>-associated peaks are obtained in the CV-treated Cu electrode which could be related to the formation of different final products (Figure 5c).

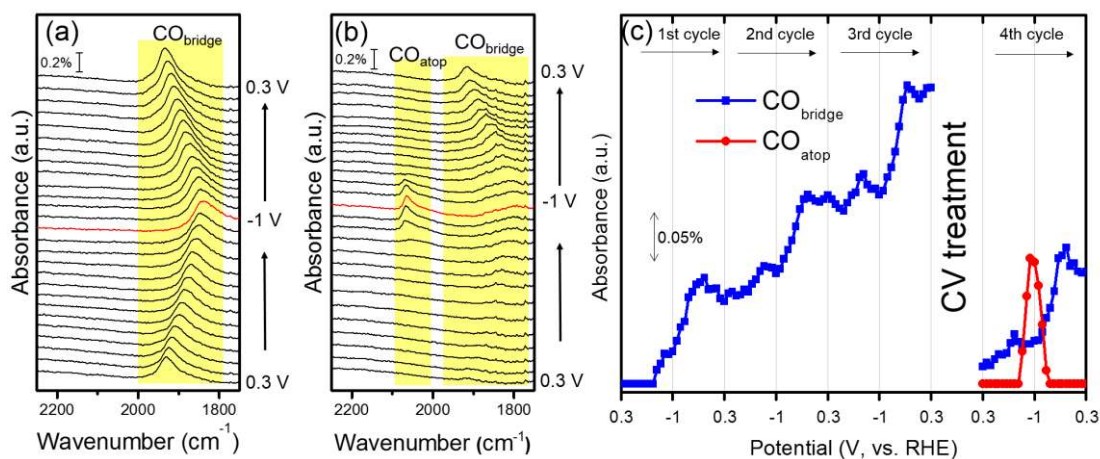


**Figure 6.** *In situ* SEIRA spectra of (a) as-prepared Cu electrode obtained in the (a) 3rd cycle and the (b) 4th cycle of CO<sub>2</sub> reduction process (after CV-treated cycles). (c) Potential-dependence of intensity of CO<sub>bridge</sub> and CO<sub>atop</sub>-associated peaks during four cycles.

We next study the formation of CO<sub>bridge</sub> and CO<sub>atop</sub> species during continuous cycles. Figure 6a-b shows the *in situ* SEIRAS of as-prepared Cu electrode obtained in the 3rd cycle and the 4th cycle of CO<sub>2</sub> reduction process (after CV-treated cycles). The reference spectrum is obtained at 0.3 V before the CO<sub>2</sub> reduction. The CO<sub>bridge</sub>-associated peak resulted from the residual CO<sub>bridge</sub> on the Cu surface is observed at 0.3 V before the third cycle (Figure 6a). The CO<sub>bridge</sub>-associated peak redshifts during the negative scan and blueshifts during the backward scan between 0.3 V and -1 V, indicating that the adsorption behavior of residual CO<sub>bridge</sub> is the same during continuous cycles.

Figure 6c shows the potential-dependence of intensity of  $\text{CO}_{\text{bridge}}$  and  $\text{CO}_{\text{atop}}$ -associated peaks during continuous four cycles. We found that the growth of residual  $\text{CO}_{\text{bridge}}$  is facilitated by polarizing the potential below -0.5 V during  $\text{CO}_2$  reduction. The intensity of  $\text{CO}_{\text{bridge}}$ -associated peak rises at -0.5 V during negative scan and keeps increasing during backward scan until -0.3 V, suggesting that residual  $\text{CO}_{\text{bridge}}$  species is formed on the surface. The total amount of residual  $\text{CO}_{\text{bridge}}$  increases from the first to third cycle. After CV treatment, the  $\text{CO}_{\text{atop}}$ -associated peak appears during the  $\text{CO}_2$  reduction, which could be related to the formation of Cu(I). The intensity of  $\text{CO}_{\text{bridge}}$ -associated peak drops, suggesting that  $\text{CO}_{\text{bridge}}$  can be removed from Cu surface during Cu oxidation process.<sup>27</sup>

Possible reasons for the growth of residual  $\text{CO}_{\text{bridge}}$  during cycles are proposed as followings. (1) The increase in surface roughness of Cu electrode could provide more surface area for  $\text{CO}_{\text{bridge}}$  adsorption during cycling. Although AFM images show that the surface roughness of as-prepared Cu electrodes is similar before and after three CV-treated cycles in the potential range of -0.3 and 0.55 V (Fig. 1b-c), the surface reconstruction of as-prepared Cu electrode could only take place at the atomic level. In addition, AFM image of the surface morphology of CV-treated Cu electrode (after 100 CV-treated cycles) shows that the surface becomes rougher. (Fig. S11) (2) *In situ* SEIRA spectra of Cu electrodes show that the peaks associated with  $\delta_{\text{HOH}}$  bending mode of

adsorbed water appear during the negative scan and maintain during the backward scan,<sup>35</sup> which is most likely due to the irreversible changes of the Cu surface. (3) The increase in the amount of residual  $\text{CO}_{\text{bridge}}$  is similar during each cycle, suggesting that  $\text{CO}_{\text{bridge}}$  species occupy a portion of Cu surface. Polycrystalline Cu electrode reconstructs and forms Cu (111) and Cu (100) facets in the electrolyte<sup>55-56</sup> and CO-induced surface reconstruction has been reported.<sup>47</sup> Thus, the irreversible surface reconstruction could lead to form more favorable sites for  $\text{CO}_{\text{bridge}}$  adsorption during cycling.

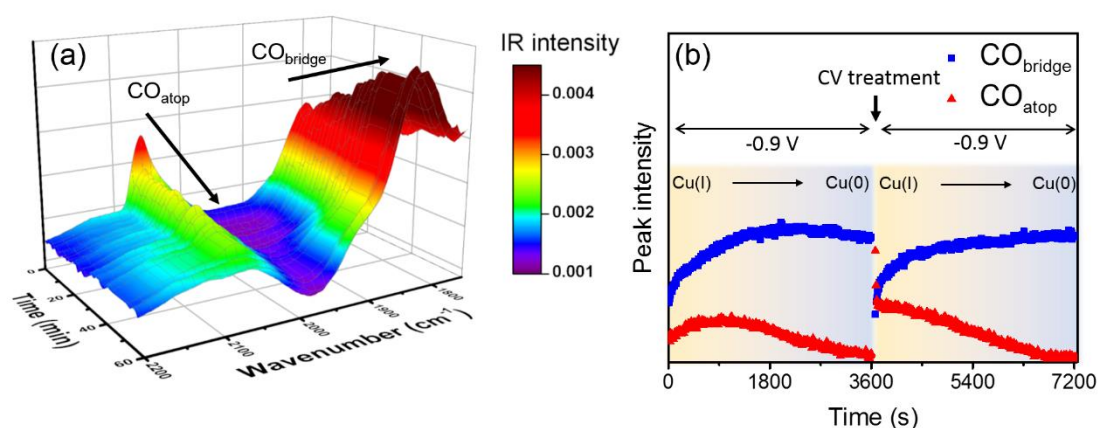


**Figure 7.** (a) *In situ* SEIRA spectra of CV-treated Cu electrode and (b) time dependence of the  $\text{CO}_{\text{bridge}}$  and  $\text{CO}_{\text{atop}}$ -associated peak intensities at -0.9 V.

In order to study the persistence of the different CO species during  $\text{CO}_2$  reduction, we examined the SEIRA spectra of CV-treated Cu electrode obtained with time, during a holding-potential at -0.9 V. Figure 7a shows the *in situ* SEIRA spectra of CV-treated Cu electrode and that obtained after holding the potential at -0.9 V for 60 min. The  $\text{CO}_{\text{bridge}}$  and  $\text{CO}_{\text{atop}}$ -associated peaks are absent at 0.3 V and these peaks appear after

stepping the potential from 0.3 to -0.9 V. Figure 7b shows the time dependence of the  $\text{CO}_{\text{bridge}}$  and  $\text{CO}_{\text{atop}}$ -associated peak intensities at -0.9 V. The intensity of  $\text{CO}_{\text{bridge}}$ -associated peak reaches maximum in  $\sim 30$  min and remains at -0.9 V. In contrast, the intensity of  $\text{CO}_{\text{atop}}$ -associated peak increases in the first 15 min and then decreases with the time. The decrease in the intensity of  $\text{CO}_{\text{atop}}$  suggests that  $\text{CO}_{\text{atop}}$  leaves the surface easily and  $\text{CO}_{\text{atop}}$  adsorption is a dynamic process. The XAS of CV-treated Cu electrode obtained during a potential hold at -0.9 V mainly exhibit Cu(I) feature for the first 15 min which is due to the slow reduction of Cu(I). After holding the potential at -0.9 V for 60 min, the oxidation state of Cu surface changes from Cu(I) to Cu(0).

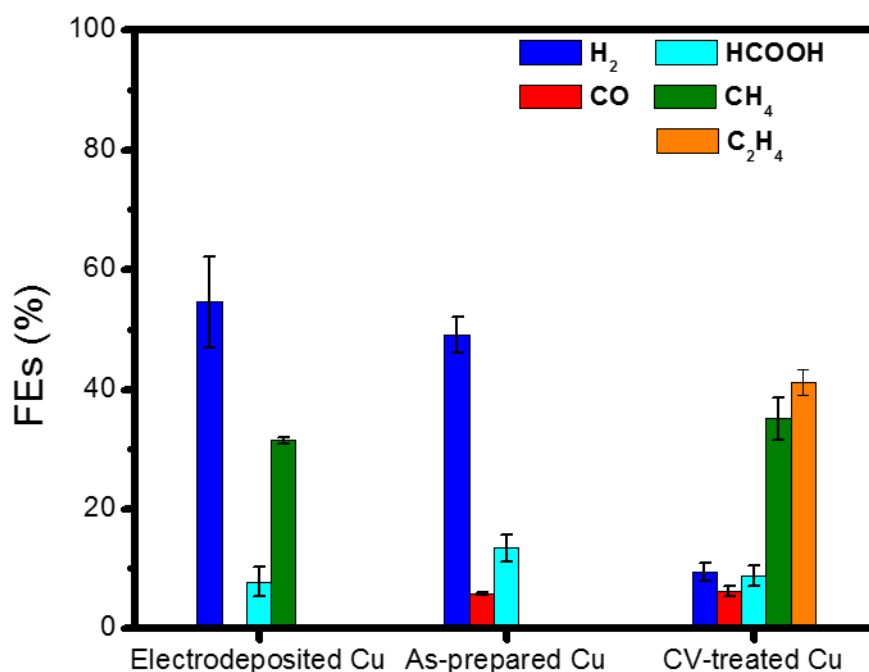


**Figure 8.** FEs of major products catalyzed by electrodeposited Cu electrode, as-prepared Cu electrode and CV-treated Cu electrode (after 100 CV-treated cycles) at -1



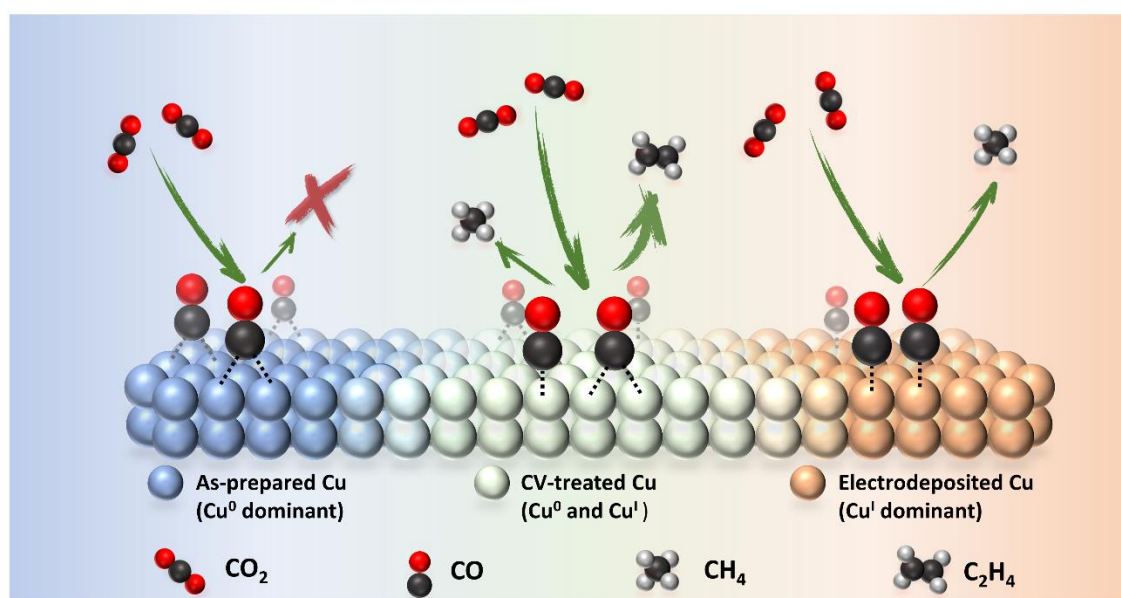
V in CO<sub>2</sub> saturated 0.1 M KHCO<sub>3</sub> electrolyte.

The product distributions obtained from various Cu catalysts were used to examine the electrocatalytic properties of Cu and gain more insight into the CO<sub>2</sub> reduction mechanism. Figure 8 shows the FEs of major products catalyzed by electrodeposited Cu electrode, as-prepared Cu electrode and CV-treated Cu electrode (after 100 CV-treated cycles) at -1 V. The major products catalyzed by electrodeposited Cu electrode at -1 V are H<sub>2</sub>, CH<sub>4</sub> and HCOOH with the FEs of 50 %, 30 % and 10 %, respectively. In addition, only small amount of C<sub>2</sub> product such as C<sub>2</sub>H<sub>4</sub> can be produced at even higher overpotential, which is consistent with previous studies.<sup>25</sup>

The major CO<sub>2</sub> reduction products over the as-prepared Cu electrode are H<sub>2</sub>, CO and HCOOH at -1 V, with the FEs being 50 %, 5 %, and 10 % at -1 V, respectively. H<sub>2</sub> becomes the dominant product, indicating that the high FE toward hydrogen evolution reaction is observed in as-prepared Cu electrode and less hydrocarbon products can be formed. In order to provide a significant effect of CV treatment on the final product analysis, the CV-treated Cu electrode is prepared after 100 CV-treated cycles for the on-line GC measurements. The CV-treated Cu electrode (after 100 CV-treated cycles) produces more hydrocarbon species such as C<sub>2</sub>H<sub>4</sub> (FE= 40 %) and CH<sub>4</sub> (FE= 35 %), suggesting that the presence of CO<sub>bridge</sub> and CO<sub>atop</sub> leads to form different products. The improved selectivity can be observed even with less CV-treated cycles (Figure S12).

In addition, similar FE of HCOOH is obtained over the three Cu catalysts at -1 V,

suggesting that the oxidation state of Cu and formation of CO species could have less effect on the formation of HCOOH.<sup>13</sup> The lower total FE (~65 %) of major products obtained in the as-prepared Cu electrode could result from the formation of residual CO (CO<sub>bridge</sub>) on as-prepared Cu surface at -1 V shown in Figure 7. The CV-treated Cu electrode with the coexistence of Cu(I) and Cu(0) results in the formation of CH<sub>4</sub> and C<sub>2</sub>H<sub>4</sub> at -1 V. Both CH<sub>4</sub> (FE= 35 %) and C<sub>2</sub>H<sub>4</sub> (FE= 40 %) are primary CO<sub>2</sub> reduction products and the FE of H<sub>2</sub> dramatically decreases to ~10 %.



**Scheme 1.** Schematic illustration of electrochemical CO<sub>2</sub> reduction on Cu surface.

We next discuss the possible reasons for the improved CO<sub>2</sub> reduction catalyzed by CV-treated Cu electrode. Previous studies showed that C<sub>2</sub> products are favored on dendritic or branched copper materials.<sup>11,14</sup> The branched copper oxide nanoparticles exhibited a high FE of ethylene (FE= 70%) and a hydrogen FE of 30% without any byproducts in a neutral aqueous solution.<sup>11</sup> Also, the surface morphology of Cu

electrode has been proposed to change the CO<sub>2</sub> reduction pathway. The surface reorganization of Cu(polycrystalline) surface to Cu(polycrystalline)-[Cu(100)] surface is a general phenomenon at the negative potential<sup>55-56</sup> and Cu(100) surface requires the lower overpotential to reduce CO<sub>2</sub> to C<sub>2</sub>H<sub>4</sub>.<sup>57-58</sup> However, the CV-treated Cu electrode exhibits similar surface morphology before and after CO<sub>2</sub> reduction (Fig. 1c, Fig. S11 and Fig. S13). Fig. S14 shows that the FEs of methane and ethylene products catalyzed by CV-treated Cu electrode (after three CV-treated cycles) decrease with the time after holding the potential at -1 V. The decreases in the product selectivity with time are not consistent with surface reorganization of Cu(100) for favorable CO<sub>2</sub>-to-ethylene conversion. Moreover, the product distributions obtained in the CV-treated Cu catalysts and dendritic or branched copper materials are different. Thus, the product distributions are not fully correlated with the changes in surface morphology in the present study.

The role of Cu oxidation state has been examined in the product selectivity. We prepared Cu electrodes with the oxidation state of Cu(0) (*i.e.*, as-prepared Cu electrode), Cu(I) (*i.e.*, electrodeposited Cu electrode) and the mixture of Cu(0) and Cu(I) (*i.e.*, CV-treated Cu electrode) in the present study. The proposed electrochemical CO<sub>2</sub> reduction mechanism on different Cu catalysts is shown in scheme 1. *In situ* SEIRA spectra show that different CO species are formed on these Cu surfaces. The electrodeposited Cu electrode shows that Cu(I) is the dominant. CO<sub>atop</sub> intermediate species is obtained over

electrodeposited Cu electrode, which could lead to form CH<sub>4</sub> as the C<sub>1</sub> product. The residual CO<sub>bridge</sub> and less hydrocarbon product are obtained in the as-prepared Cu electrode with Cu(0). In the CV-treated Cu electrode, XAS show the combination of Cu(I) and Cu(0) feature. The presence of both CO<sub>atop</sub> and CO<sub>bridge</sub> intermediate species on Cu surface is observed and the formation of C<sub>2</sub> products such as C<sub>2</sub>H<sub>4</sub> is enhanced. Although surface-adsorbed CO<sub>bridge</sub> has been considered as the irreversible CO species, which is inert to the reduction reaction,<sup>27</sup> our results suggest that CO<sub>bridge</sub> might play an important role in producing the C<sub>2</sub> products in the presence of CO<sub>atop</sub>. Quantum mechanics method was used to validate a unique catalyst for electrochemical CO<sub>2</sub> reduction.<sup>23</sup> Xiao et al. proposed that the selectivity and activity of C<sub>2</sub> products are enhanced at the borders of oxidized and metallic surface regions.<sup>23</sup> Based on their proposed model, two CO species including CO<sub>bridge</sub> and CO<sub>atop</sub> adsorbed on Cu(0) and Cu(I) regions are negatively and positively charged, respectively, which assist the CO dimerization and form valuable chemicals products (HCO<sub>x</sub>). Thus, the theoretical model might correlate with the coexistence of CO<sub>bridge</sub> and CO<sub>atop</sub> intermediates for the improved formation of C<sub>2</sub> product in the CV-treated Cu electrode.

## Conclusions

In summary, we found that the Cu surface with oxidation state distribution changes the CO<sub>2</sub> reduction mechanism. The electrodeposited Cu electrode shows more Cu(I).

The  $\text{CO}_{\text{atop}}$  intermediate species is formed on the surface and the formation of  $\text{C}_1$  hydrocarbon product is obtained during further reduction. As-prepared Cu electrode exhibits the oxidation state of Cu(0). The  $\text{CO}_{\text{bridge}}$  is formed on the surface and inhibits the formation of hydrocarbon product. In contrast, the CV-treated Cu electrode shows the coexistence of Cu(I) and Cu(0) and forms both  $\text{CO}_{\text{atop}}$  and  $\text{CO}_{\text{bridge}}$  during  $\text{CO}_2$  reduction. The enhanced  $\text{C}_2$  product selectivity is also obtained. Thus, oxidation state of Cu catalysts affects the electrocatalytic properties of interface and modulates the  $\text{CO}_2$  reduction mechanism. Our findings provide a strategy for designing more selective Cu electrocatalysts for electrochemical  $\text{CO}_2$  reduction.

## ASSOCIATED CONTENT

### **Supporting Information.**

AFM images of as-prepared Cu and the cross section profile of as-prepared Cu (Figure S1). AFM image and CV of electrodeposited Cu electrode (Figure S2). Cell configuration of in situ SEIRAS measurements (Figure S3). Cell configuration of in situ soft XAS measurements (Figure S4). Cell configuration of on-line GC measurements (Figure S5). Double layer capacitances of as-prepared Cu electrode and CV-treated Cu electrode (Figure S6). EXAFS spectra of pristine as-prepared, CV-

treated and electrodeposited Cu electrodes (Figure S7). Cu L<sub>3</sub>-edge XAS of standard Cu electrodes in TFY mode (Figure S8). *In situ* SEIRA spectra of electrodeposited Cu electrode, as-prepared Cu electrode and CV-treated Cu electrode (Figure S9). *In situ* SEIRA spectra of CV-treated Cu electrode obtained at -1 V and without applied potential (Figure S10). AFM image of the surface morphology of CV-treated Cu electrode (after 100 CV-treated cycles) (Figure S11). FEs of major products catalyzed by CV-treated Cu electrode (after 3, 10 and 30 CV-treated cycles) at -1 V (Figure S12). AFM images of the surface morphology of (a) CV-treated Cu electrode (3 CV-treated cycles) and (b) CV-treated Cu electrode (100 CV-treated cycles) after holding the potential at -1 V for 60 min in the CO<sub>2</sub> saturated 0.1 M KHCO<sub>3</sub> electrolyte (Figure S13). FEs of methane and ethylene catalyzed by CV-treated Cu electrode (after three CV-treated cycles) after holding the potential at -1 V in CO<sub>2</sub> saturated 0.1 M KHCO<sub>3</sub> electrolyte. (Figure S14). This material is available free of charge via the Internet at <http://pubs.acs.org>.

## AUTHOR INFORMATION

### Corresponding Authors

\*Email: [hengliangwu@ntu.edu.tw](mailto:hengliangwu@ntu.edu.tw)

Telephone: +886-2-33665260

## Notes

The authors declare no competing financial interest.

## Acknowledgments

This research was funded by MOST (Ministry of Science and Technology), Taiwan. (107-2113-M-002 -014 -MY2) We thank Prof. Tsan-Yao Chen in Department of Engineering and System Science, National Tsing Hua University and Prof. Kuan-Wen Wang in Institute of Materials Science and Engineering, National Central University for the technical support. We thank Ms. Po-Yu Su in Center for Condensed Matter Sciences, National Taiwan University for the gas product measurements. We thank financial support from the Center of Atomic Initiative for New Materials, National Taiwan University, from the Featured Areas Research Center Program within the framework of the Higher Education Sprout Project by the Ministry of Education in Taiwan (108L9008).

## References

1. Seh, Z. W.; Kibsgaard, J.; Dickens, C. F.; Chorkendorff, I. B.; Norskov, J. K.; Jaramillo, T. F., Combining theory and experiment in electrocatalysis: Insights into materials design. *Science* **2017**, *355*, eaad4998.
2. Zhu, D. D.; Liu, J. L.; Qiao, S. Z., Recent Advances in Inorganic Heterogeneous Electrocatalysts for Reduction of Carbon Dioxide. *Adv. Mater.* **2016**, *28*, 3423.
3. Kas, R.; Kortlever, R.; Milbrat, A.; Koper, M. T. M.; Mul, G.; Baltrusaitis, J., Electrochemical CO<sub>2</sub> reduction on Cu<sub>2</sub>O-derived copper nanoparticles: controlling the

- catalytic selectivity of hydrocarbons. *PCCP* **2014**, *16*, 12194.
- Gao, D. F.; Aran-Ais, R. M.; Jeon, H. S.; Cuenya, B. R., Rational catalyst and electrolyte design for CO<sub>2</sub> electroreduction towards multicarbon products. *Nat. Catal.* **2019**, *2*, 198.
  - Khezri, B.; Fisher, A. C.; Pumera, M., CO<sub>2</sub> reduction: the quest for electrocatalytic materials. *J. Mater. Chem. A* **2017**, *5*, 8230.
  - Zheng, Y.; Vasileff, A.; Zhou, X. L.; Jiao, Y.; Jaroniec, M.; Qiao, S. Z., Understanding the Roadmap for Electrochemical Reduction of CO<sub>2</sub> to Multi-Carbon Oxygenates and Hydrocarbons on Copper-Based Catalysts. *J. Am. Chem. Soc.* **2019**, *141*, 7646.
  - Takahashi, I.; Koga, O.; Hoshi, N.; Hori, Y., Electrochemical reduction of CO<sub>2</sub> at copper single crystal Cu(S)-[n (111) x (111)] and Cu(S)-[n (110) x (100)] electrodes. *J. Electroanal. Chem.* **2002**, *533*, 135.
  - Hori, Y.; Takahashi, I.; Koga, O.; Hoshi, N., Electrochemical reduction of carbon dioxide at various series of copper single crystal electrodes. *J. Mol. Catal. A: Chem.* **2003**, *199*, 39.
  - Reske, R.; Mistry, H.; Behafarid, F.; Roldan Cuenya, B.; Strasser, P., Particle Size Effects in the Catalytic Electroreduction of CO<sub>2</sub> on Cu Nanoparticles. *J. Am. Chem. Soc.* **2014**, *136*, 6978.
  - Cheng, T.; Xiao, H.; Goddard, W. A., Nature of the Active Sites for CO Reduction on Copper Nanoparticles; Suggestions for Optimizing Performance. *J. Am. Chem. Soc.* **2017**, *139*, 11642.
  - Kim, J.; Choi, W.; Park, J. W.; Kim, C.; Kim, M.; Song, H., Branched Copper Oxide Nanoparticles Induce Highly Selective Ethylene Production by Electrochemical Carbon Dioxide Reduction. *J. Am. Chem. Soc.* **2019**, *141*, 6986.
  - Jung, H.; Lee, S. Y.; Lee, C. W.; Cho, M. K.; Won, D. H.; Kim, C.; Oh, H. S.; Min, B. K.; Hwang, Y. J., Electrochemical Fragmentation of Cu<sub>2</sub>O Nanoparticles Enhancing Selective C-C Coupling from CO<sub>2</sub> Reduction Reaction. *J. Am. Chem. Soc.* **2019**, *141*, 4624.
  - Gao, D. F.; Zegkinoglou, I.; Divins, N. J.; Scholten, F.; Sinev, I.; Grosse, P.; Roldan Cuenya, B., Plasma-Activated Copper Nanocube Catalysts for Efficient Carbon Dioxide Electroreduction to Hydrocarbons and Alcohols. *ACS Nano* **2017**, *11*, 4825.
  - Scholten, F.; Sinev, I.; Bernal, M.; Cuenya, B. R., Plasma-Modified Dendritic Cu Catalyst for CO<sub>2</sub> Electroreduction. *ACS Catal.* **2019**, *9*, 5496.
  - Eilert, A.; Cavalca, F.; Roberts, F. S.; Osterwalder, J.; Liu, C.; Favaro, M.; Crumlin, E. J.; Ogasawara, H.; Friebel, D.; Pettersson, L. G. M.; Nilsson, A., Subsurface Oxygen in Oxide-Derived Copper Electrocatalysts for Carbon Dioxide Reduction. *J. Phys. Chem. Lett.* **2017**, *8*, 285.



16. Dinh, C. T.; Burdyny, T.; Kibria, M. G.; Seifitokaldani, A.; Gabardo, C. M.; de Arquer, F. P. G.; Kiani, A.; Edwards, J. P.; De Luna, P.; Bushuyev, O. S.; Zou, C. Q.; Quintero-Bermudez, R.; Pang, Y. J.; Sinton, D.; Sargent, E. H., CO<sub>2</sub> electroreduction to ethylene via hydroxide-mediated copper catalysis at an abrupt interface. *Science* **2018**, *360*, 783.
17. Favaro, M.; Xiao, H.; Cheng, T.; Goddard, W. A.; Yano, J.; Crumlin, E. J., Subsurface oxide plays a critical role in CO<sub>2</sub> activation by Cu(111) surfaces to form chemisorbed CO<sub>2</sub>, the first step in reduction of CO<sub>2</sub>. *Proc. Natl. Acad. Sci. U.S.A.* **2017**, *114*, 6706.
18. Mistry, H.; Varela, A. S.; Bonifacio, C. S.; Zegkinoglou, I.; Sinev, I.; Choi, Y. W.; Kisslinger, K.; Stach, E. A.; Yang, J. C.; Strasser, P.; Cuenya, B. R., Highly selective plasma-activated copper catalysts for carbon dioxide reduction to ethylene. *Nat. Comm.* **2016**, *7*, 12123.
19. Li, C. W.; Kanan, M. W., CO<sub>2</sub> Reduction at Low Overpotential on Cu Electrodes Resulting from the Reduction of Thick Cu<sub>2</sub>O Films. *J. Am. Chem. Soc.* **2012**, *134*, 7231.
20. Eilert, A.; Roberts, F. S.; Friebel, D.; Nilsson, A., Formation of Copper Catalysts for CO<sub>2</sub> Reduction with High Ethylene/Methane Product Ratio Investigated with *In Situ* X-ray Absorption Spectroscopy. *J. Phys. Chem. Lett.* **2016**, *7*, 1466.
21. Mariano, R. G.; McKelvey, K.; White, H. S.; Kanan, M. W., Selective increase in CO<sub>2</sub> electroreduction activity at grain-boundary surface terminations. *Science* **2017**, *358*, 1187.
22. Feng, X. F.; Jiang, K. L.; Fan, S. S.; Kanan, M. W., Grain-Boundary-Dependent CO<sub>2</sub> Electroreduction Activity. *J. Am. Chem. Soc.* **2015**, *137*, 4606.
23. Xiao, H.; Goddard, W. A.; Cheng, T.; Liu, Y. Y., Cu metal embedded in oxidized matrix catalyst to promote CO<sub>2</sub> activation and CO dimerization for electrochemical reduction of CO<sub>2</sub>. *Proc. Natl. Acad. Sci. U.S.A.* **2017**, *114*, 6685.
24. Heyes, J.; Dunwell, M.; Xu, B. J., CO<sub>2</sub> Reduction on Cu at Low Overpotentials with Surface-Enhanced *in Situ* Spectroscopy. *J. Phys. Chem. C* **2016**, *120*, 17334.
25. Wuttig, A.; Liu, C.; Peng, Q. L.; Yaguchi, M.; Hendon, C. H.; Motobayashi, K.; Ye, S.; Osawa, M.; Surendranath, Y., Tracking a Common Surface-Bound Intermediate during CO<sub>2</sub>-to-Fuels Catalysis. *ACS Cent. Sci.* **2016**, *2*, 522.
26. Zhu, S. Q.; Jiang, B.; Cai, W. B.; Shao, M. H., Direct Observation on Reaction Intermediates and the Role of Bicarbonate Anions in CO<sub>2</sub> Electrochemical Reduction Reaction on Cu Surfaces. *J. Am. Chem. Soc.* **2017**, *139*, 15664.
27. Gunathunge, C. M.; Ovalle, V. J.; Li, Y. W.; Janik, M. J.; Waagele, M. M., Existence of an Electrochemically Inert CO Population on Cu Electrodes in Alkaline pH. *ACS Catal.* **2018**, *8*, 7507.
28. Malkani, A. S.; Dunwell, M.; Xu, B. J., Operando Spectroscopic Investigations of

Copper and Oxide Derived Copper Catalysts for Electrochemical CO Reduction. *ACS Catal.* **2019**, *9*, 474.

29. Hayden, B. E.; Kretzschmar, K.; Bradshaw, A. M., An Infrared Spectroscopic Study of CO on Cu(111) - the Linear, Bridging and Physisorbed Species. *Surf. Sci.* **1985**, *155*, 553.

30. Salimon, J.; Hernandez-Romero, R. M.; Kalaji, M., The dynamics of the conversion of linear to bridge bonded CO on Cu. *J. Electroanal. Chem.* **2002**, *538*, 99.

31. Ooka, H.; Figueiredo, M. C.; Koper, M. T. M., Competition between Hydrogen Evolution and Carbon Dioxide Reduction on Copper Electrodes in Mildly Acidic Media. *Langmuir* **2017**, *33*, 9307.

32. Wang, H. F.; Yan, Y. G.; Hu, S. J.; Cai, W. B.; Xu, Q. H.; Osawa, M., Seeded growth fabrication of Cu-on-Si electrodes for *in situ* ATR-SEIRAS applications. *Electrochim. Acta* **2007**, *52*, 5950.

33. Lee, S.; Lee, J., Ethylene Selectivity in CO Electroreduction when using Cu Oxides: An *In Situ* ATR-SEIRAS Study. *ChemElectroChem* **2018**, *5*, 558.

34. Yaguchi, M.; Uchida, T.; Motobayashi, K.; Osawa, M., Speciation of Adsorbed Phosphate at Gold Electrodes: A Combined Surface-Enhanced Infrared Absorption Spectroscopy and DFT Study. *J. Phys. Chem. Lett.* **2016**, *7*, 3097.

35. Ataka, K.; Yotsuyanagi, T.; Osawa, M., Potential-dependent reorientation of water molecules at an electrode/electrolyte interface studied by surface-enhanced infrared absorption spectroscopy. *J. Phys. Chem.* **1996**, *100*, 10664.

36. Chen, Y. X.; Miki, A.; Ye, S.; Sakai, H.; Osawa, M., Formate, an active intermediate for direct oxidation of methanol on Pt electrode. *J. Am. Chem. Soc.* **2003**, *125*, 3680.

37. Velasco-Velez, J. J.; Jones, T.; Gao, D.; Carbonio, E.; Arrigo, R.; Hsu, C. J.; Huang, Y. C.; Dong, C. L.; Chen, J. M.; Lee, J. F.; Strasser, P.; Cuenya, B. R.; Schlogl, R.; Knop-Gericke, A.; Chuang, C. H., The Role of the Copper Oxidation State in the Electrocatalytic Reduction of CO<sub>2</sub> into Valuable Hydrocarbons. *ACS Sustain. Chem. Eng.* **2019**, *7*, 1485.

38. Degroot, F. M. F., X-Ray-Absorption and Dichroism of Transition-Metals and Their Compounds. *J. Electron. Spectrosc. Relat. Phenom.* **1994**, *67*, 529.

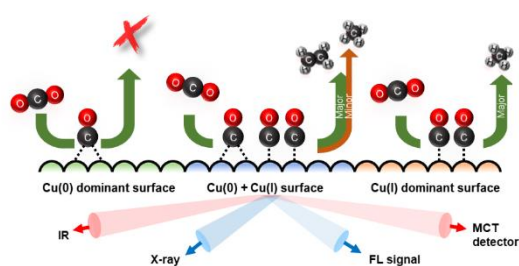
39. Achkar, A. J.; Regier, T. Z.; Wadati, H.; Kim, Y. J.; Zhang, H.; Hawthorn, D. G., Bulk sensitive X-ray absorption spectroscopy free of self-absorption effects. *Phys. Rev. B* **2011**, *83*, 081106.

40. Velasco-Velez, J. J.; Skorupska, K.; Frei, E.; Huang, Y. C.; Dong, C. L.; Su, B. J.; Hsu, C. J.; Chou, H. Y.; Chen, J. M.; Strasser, P.; Schlogl, R.; Knop-Gericke, A.; Chuang, C. H., The Electro-Deposition/Dissolution of CuSO<sub>4</sub> Aqueous Electrolyte Investigated by *In Situ* Soft X-ray Absorption Spectroscopy. *J. Phys. Chem. B* **2018**, *122*, 780.

41. Lien, H. T.; Wong, D. P.; Tsao, N. H.; Huang, C. I.; Su, C. C.; Chen, K. H.; Chen, L. C., Effect of Copper Oxide Oxidation State on the Polymer-Based Solar Cell Buffer Layers. *ACS Appl. Mater. Inter.* **2014**, *6*, 22445.
42. Hollmark, H. M.; Vegelius, J. R.; Kristiansen, P.; Werme, L.; Duda, L. C., Exposure of Oxidized Copper Surfaces to Aqueous Na<sub>2</sub>S Solution Studied with Soft X-Ray Spectroscopy. *J. Electrochem. Soc.* **2011**, *158*, C1.
43. Stern, E. A.; Kim, K., Thickness Effect on the Extended-X-Ray-Absorption-Fine-Structure Amplitude. *Phys. Rev. B* **1981**, *23*, 3781.
44. Wang, X. T.; Martin, N. M.; Nilsson, J.; Carlson, S.; Gustafson, J.; Skoglundh, M.; Carlsson, P. A., Copper-Modified Zeolites and Silica for Conversion of Methane to Methanol. *Catalysts* **2018**, *8*, 545.
45. Weng, Z.; Wu, Y. S.; Wang, M. Y.; Jiang, J. B.; Yang, K.; Huo, S. J.; Wang, X. F.; Ma, Q.; Brudvig, G. W.; Batista, V. S.; Liang, Y. Y.; Feng, Z. X.; Wang, H. L., Active sites of copper-complex catalytic materials for electrochemical carbon dioxide reduction. *Nat. Comm.* **2018**, *9*, 415.
46. Ruosi, A.; Raisch, C.; Verna, A.; Werner, R.; Davidson, B. A.; Fujii, J.; Kleiner, R.; Koelle, D., Electron sampling depth and saturation effects in perovskite films investigated by soft x-ray absorption spectroscopy. *Phys. Rev. B* **2014**, *90*, 125120.
47. Gunathunge, C. M.; Li, X.; Li, J. Y.; Hicks, R. P.; Ovalle, V. J.; Waegele, M. M., Spectroscopic Observation of Reversible Surface Reconstruction of Copper Electrodes under CO<sub>2</sub> Reduction. *J. Phys. Chem. C* **2017**, *121*, 12337.
48. Sun, S. G.; Cai, W. B.; Wan, L. J.; Osawa, M., Infrared absorption enhancement for CO adsorbed on Au films in perchloric acid solutions and effects of surface structure studied by cyclic voltammetry, scanning tunneling microscopy, and surface-enhanced IR spectroscopy. *J. Phys. Chem. B* **1999**, *103*, 2460.
49. Samjeske, G.; Komatsu, K.; Osawa, M., Dynamics of CO Oxidation on a Polycrystalline Platinum Electrode: A Time-Resolved Infrared Study. *J. Phys. Chem. C* **2009**, *113*, 10222.
50. Iwasita, T.; Nart, F. C.; Lopez, B.; Vielstich, W., On the Study of Adsorbed Species at Platinum from Methanol, Formic-Acid and Reduced Carbon-Dioxide Via *In situ* Ft-Ir Spectroscopy. *Electrochim. Acta* **1992**, *37*, 2361.
51. Figueiredo, M. C.; Ledezma-Yanez, I.; Koper, M. T. M., *In Situ* Spectroscopic Study of CO<sub>2</sub> Electroreduction at Copper Electrodes in Acetonitrile. *ACS Catal.* **2016**, *6*, 2382.
52. Osawa, M.; Ataka, K.; Yoshii, K.; Nishikawa, Y., Surface-Enhanced Infrared-Spectroscopy - The Origin of the Absorption Enhancement and Band Selection Rule in the Infrared-Spectra of Molecules Adsorbed on Fine Metal Particles. *Appl. Spectrosc.* **1993**, *47*, 1497.

53. Lee, S. J.; Han, S. W.; Yoon, M.; Kim, K., Adsorption characteristics of 4-dimethylaminobenzoic acid on silver and titania: Diffuse reflectance infrared Fourier transform spectroscopy study. *Vib. Spectrosc.* **2000**, *24*, 265.
54. Firet, N. J.; Smith, W. A., Probing the Reaction Mechanism of CO<sub>2</sub> Electroreduction over Ag Films via Operando Infrared Spectroscopy. *ACS Catal.* **2017**, *7*, 606.
55. Kim, Y. G.; Baricuatro, J. H.; Javier, A.; Gregoire, J. M.; Soriaga, M. P., The Evolution of the Polycrystalline Copper Surface, First to Cu(111) and Then to Cu(100), at a Fixed CO<sub>2</sub>RR Potential: A Study by Operand EC-STM. *Langmuir* **2014**, *30*, 15053.
56. Kim, Y.-G.; Baricuatro, J. H.; Soriaga, M. P., Surface Reconstruction of Polycrystalline Cu Electrodes in Aqueous KHCO<sub>3</sub> Electrolyte at Potentials in the Early Stages of CO<sub>2</sub> Reduction. *Electrocatalysis* **2018**, *9*, 526.
57. Huang, Y.; Handoko, A. D.; Hirunsit, P.; Yeo, B. S., Electrochemical Reduction of CO<sub>2</sub> Using Copper Single-Crystal Surfaces: Effects of CO\* Coverage on the Selective Formation of Ethylene. *ACS Catal.* **2017**, *7*, 1749.
58. Schouten, K. J.; Qin, Z.; Perez Gallent, E.; Koper, M. T., Two pathways for the formation of ethylene in CO reduction on single-crystal copper electrodes. *J. Am. Chem. Soc.* **2012**, *134*, 9864.

### Table of Contents (TOC) graphic



“For Table of Contents Only”